STRUCTURAL BIOLOGY COMMUNICATIONS

ISSN 2053-230X

Crystallization and low-resolution structure solution of the SALM3–PTPσ synaptic adhesion complex

Sudeep Karki and Tommi Kajander*

Institute of Biotechnology, Helsinki Institute of Life Sciences, University of Helsinki, Viikinkaari 1, 00014 Helsinki, Finland. *Correspondence e-mail: tommi.kajander@helsinki.fi

Received 12 October 2021
Accepted 3 December 2021

Edited by J. Newman, Bio21 Collaborative Crystallisation Centre, Australia

Keywords: synaptic adhesion; SALM3; protein tyrosine phosphatases; protein complex; crystallization.

Supporting information: this article has supporting information at journals.iucr.org/f

Synaptic adhesion molecules are major organizers of the neuronal network and play a crucial role in the regulation of synapse development and maintenance in the brain. Synaptic adhesion-like molecules (SALMs) and leukocyte common antigen-related receptor protein tyrosine phosphatases (LAR-PTPs) are adhesion protein families with established synaptic function. Dysfunction of several synaptic adhesion molecules has been linked to cognitive disorders such as autism spectrum disorders and schizophrenia. A recent study of the binding and complex structure of SALM3 and PTPσ using small-angle X-ray scattering revealed a 2:2 complex similar to that observed for the interaction of human SALM5 and PTPδ However, the molecular structure of the SALM3–PTPσ complex remains to be determined beyond the small-angle X-ray scattering model. Here, the expression, purification, crystallization and initial 6.5 Å resolution structure of the mouse SALM3–PTPσ complex are reported, which further verifies the formation of a 2:2 trans-heterotetrameric complex similar to the crystal structure of human SALM5–PTPδ and validates the architecture of the previously reported small-angle scattering-based solution structure of the SALM3–PTPσ complex. Details of the protein expression and purification, crystal optimization trials, and the initial structure solution and data analysis are provided.

1. Introduction

Synaptic adhesion molecules are major organizers of neuronal network contacts, which are localized at the presynaptic and postsynaptic cell membranes at the synaptic cleft, and play a crucial role in the regulation of synapse development and maintenance in the brain (Missler *et al.*, 2012; Yamagata *et al.*, 2003). Neurexins (Ushkaryov *et al.*, 1992; Reissner *et al.*, 2013), neuroligins (Craig & Kang, 2007), synaptic adhesion-like molecules (SALMs; Craig & Kang, 2007; Ko *et al.*, 2006), leucine-rich repeat (LRR) transmembrane neuronal proteins (LRRTMs; Laurén *et al.*, 2003), leukocyte common antigen-related receptor protein tyrosine phosphatases (LAR-PTPs; Laurén *et al.*, 2003; Um & Ko, 2013) and netrin-G ligands (NGLs; Seiradake *et al.*, 2011) are among the protein families of synaptic adhesion molecules with established synaptic function. Dysfunction of several synaptic adhesion molecules has been linked to cognitive disorders such as autism spectrum disorders and schizophrenia (Yamagata *et al.*, 2003; Leshchyns'ka & Sytnyk, 2016; Medina-Cano *et al.*, 2018; Gorlewicz & Kaczmarek, 2018).

The SALM proteins form a family of LRR-containing synaptic adhesion molecules which has five known members (SALM1–SALM5; Ko *et al.*, 2006). All of the SALM proteins share a similar domain organization, with an LRR domain, an immunoglobulin (Ig) domain and a fibronectin III (FnIII)

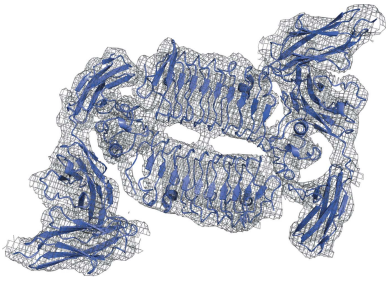

Table 1
Macromolecular cloning and expression information.

Protein	SALM3 LRR-Ig	PTPσ Ig1-3
DNA source	*Mus musculus*	*Mus musculus*
Forward primer	TTTTGAATTCTGCCCGCTACCCTGTGTGTG	TTTTGAATTCGAAGAACCACCCAGGTTTATC
Reverse primer	TTTTGGTACCCTGTAGGGCATGGCACAGGG	TTTTGGTACCTTTGGGGAGAGATTTTACAG
Expression vector	pRMHA3	pRMHA3
Expression host	*Drosophila melanogaster* S2 cell line	*Drosophila melanogaster* S2 cell line
Complete amino-acid sequence of the construct produced†	MPLLLLLPLLWAGALAMDKLEFCPLPCVCQNLSESLSTLCAHR GLLFVPPNVDRRTVELRLADNFIQALGPPDFRNMTGLVDLT LSRNAITRIGARSFGDLESLRSLHLDGNRLVELGSSSLRGP VNLQHLILSGNQLGRIAPGAFDDFLDSLEDLDVSYNNLRQV PWAGIGSMPALHTLNLDHNLIDALPPGVFAQLSQLSRLDTS NRLATLAPDPLFSRGRDAESPSPLVLSFSGNPLHCNCELLW LRRLARPDDLETCASPPTLAGRYFWAVPEGEFSCEPPLIAR HTQRLWVLEGQRATLRCRALGDPVPTMHWVGPDDRLVGNSS RAWAFPNGTLEIGVTGAGDAGAYTCIATNPAGEATARVELR VLALGTRGSLEVLFQGP**KSCDKTHTCPPCPAPELLGGPSVF LFPPKPKDTLMISRTPEVTCVVVDVSHEDPEVKFNWYVDGV EVHNAKTKPREEQYNSTYRVVSVLTVLHQDWLNGKEYKCKV SNKALPAPIEKTISKAKGQPREPQVYTLPPSRDELTKNQVS LTCLVKGFYPSDIAVEWESNGQPENNYKTTPPVLDSDGSFF LYSKLTVDKSRWQQGNVFSCSVMHEALHNHYTQKSLSLSPG K**	MPLLLLLPLLWAGALAMDKLEFEEPPRFIREPKDQIGVSGGVA SFVCQATGDPKPRVTWNKKGKKVNSQRFETIDFDESSGAVL RIQPLRTPRDENVYECVAQNSVGEITIHAKLTVLREDQLPP GFPNIDMGPQLKVVERTRTATMLCAASGNPDPEITWFKDFL PVDPSASNGRIKQLRSGALQIESSEETDQGKYECVATNSAG VRYSSPANLYVRELREVRRVAPRFSILPMSHEIMPGGNVNI TCVAVGSPMPYVKWMQGAEDLTPEDDMPVGRNVLELTDVKD SANYTCVAMSSLGVIEAVAQITVKSLPK**KGTRGS**LEVLFQG P**KSCDKTHTCPPCPAPELLGGPSVFLFPPKPKDTLMISRTP EVTCVVVDVSHEDPEVKFNWYVDGVEVHNAKTKPREEQYNS TYRVVSVLTVLHQDWLNGKEYKCKVSNKALPAPIEKTISKA KGQPREPQVYTLPPSRDELTKNQVSLTCLVKGFYPSDIAVE WESNGQPENNYKTTPPVLDSDGSFFLYSKLTVDKSRWQQGN VFSCSVMHEALHNHYTQKSLSLSPGK**

† The N-terminal CD33 signal sequence is underlined. The SALM3 LRR-Ig and PTPσ Ig1-3 sequences are shown in blue, the PreScission protein cleavage site in red and the Fc tag in bold.

domain in the extracellular region, followed by a transmembrane (TM) domain and a short cytoplasmic region. SALM1–SALM3 contain type I PDZ-binding motifs in the cytoplasmic region which are absent in SALM4 and SALM5 (Ko *et al.*, 2006; Nam *et al.*, 2011).

SALM3 promotes the differentiation of excitatory and inhibitory presynaptic structures in contacting axons via trans-synaptic interaction with LAR-PTPs (Mah *et al.*, 2010; Li *et al.*, 2015). *In vivo* studies with SALM3 knockout mice showed markedly reduced excitatory synapse numbers and locomotor activity, and behavioral hypoactivity (Li *et al.*, 2015). In a previous study, we determined the structure of the complex of SALM3 with PTPσ using small-angle X-ray scattering (SAXS), revealing a 2:2 complex similar to the human SALM5–PTPδ and SALM2–PTPδ complexes. The relevance of the key interface residues between SALM3 and PTPσ was further confirmed by mutational analysis with cellular binding assays and artificial synapse-formation assays (Karki *et al.*, 2020). However, the structural details of the SALM3–PTPσ complex remain to be resolved beyond the model based on the SAXS data.

SALM3 interacts with all three known members of the LAR-PTPs (LAR, PTPσ and PTPδ) to induce presynaptic differentiation (Li *et al.*, 2015; Karki *et al.*, 2018). The extracellular region of LAR-PTPs contains three Ig domains, 4–8 FnIII domains and multiple splicing variants at several sites: mini-exon A (meA) in the Ig2 domain, mini-exon B (meB) between the Ig2 and Ig3 domains and mini-exon C (meC) located in the FnIII domain. LAR-PTPs further contain two tandem tyrosine phosphatase domains in the cytoplasmic region that are presumably involved in regulation of presynaptic signaling (Um & Ko, 2013; Han *et al.*, 2016). The Ig domains of PTPδ and PTPσ are involved in interaction with the LRR and Ig domains of SALM3 and SALM5, and the interaction is enhanced in the presence of the LAR-PTP mini-exon B (meB) (Lin *et al.*, 2018; Choi *et al.*, 2016; Karki *et al.*, 2020).

In this study, we report the expression, purification, crystallization and initial low-resolution crystal structure of the mouse SALM3–PTPσ complex, which verifies the formation of a 2:2 trans-heterotetrameric complex similar to the crystal structure of human SALM5–PTPδ and confirms the architecture of the previously reported model of the SALM3–PTPσ complex based on SAXS data (Lin *et al.*, 2018; Karki *et al.*, 2020).

2. Materials and methods

2.1. Cloning

The cDNA for mouse SALM3 was obtained from ImaGenes GmbH and the PTPσ cDNA was a kind gift from Dr Juha Kuja-Panula. Mouse SALM3 LRR-Ig (residues 17–367; UniProtKB Q80XU8) and PTPσ Ig1-3 (residues 33–331; UniProtKB B0V251) were cloned into modified *Drosophila* pRMHA3 expression vector (Bunch *et al.*, 1988) using the EcoRI and KpnI restriction enzymes. The generated plasmid constructs contained an N-terminal CD33 signal sequence followed by the SALM3 LRR-Ig or PTPσ Ig1-3 sequence and a C-terminal Fc tag preceded by a PreScission protease-cleavage site (Table 1).

2.2. Protein expression and purification

The protein expression of SALM3 LRR-Ig and PTPσ Ig1-3 was verified by transient transfection and Western blot detection with goat anti-human polyclonal horse radish peroxidase (HRP) conjugated antibody (Abcam ab98567). Stable *Drosophila* Schneider 2 (S2) cell lines for the expres-

sion of SALM3 LRR-Ig and PTPσ Ig1-3 were generated for large-scale protein purification. HyQ-SFX medium (GE Healthcare) was used for expression of the SALM3 LRR-Ig and PTPσ Ig1-3 constructs and for the maintenance of S2 cell lines. For generation of stable cell lines of S2 cells, 1.25×10^6 cells per well were plated on a six-well plate at room temperature for 24 h. The cells were transfected with 4 µg of DNA containing the pRMHA3 expression vector mixed 20:1 with the pCoHygro selection plasmid. The DNA was diluted into 400 µl of the medium with 8 µl TransIT insect reagent (Mirus Bio LLC), and the mixture was incubated for 20 min and added to the cells. After three days, selection was started: the cells and medium were centrifuged at 1100 rev min^{-1} for 3 min and the cells were resuspended in the medium with 0.3 mg ml^{-1} hygromycin and replated into the same wells. The selection was continued for three weeks, with the medium changed every six days, in the same six-well plate. After three weeks, the cells were amplified to 0.8×10^6 cells per millitre in a total volume of 25 ml. The cells were amplified every six days until the cell viability was above 95%. The cell viability was detected by staining the cells with trypan blue with detection using an TC20TM Automated Cell Counter (Bio-Rad). For large-scale protein purification from stable cell lines, the S2 cells were divided 1:10 into HyQ-SFX medium supplemented with 0.15 mg ml^{-1} hygromycin. The cells were grown in a shaker incubator at 25°C and 100 rev min^{-1} for 24 h and were induced with 0.7 m*M* $CuSO_4$; expression was carried out for six days, after which the medium was harvested and the cells were pelleted by centrifugation at 7000 rev min^{-1} for 20 min at 4°C. The protein was affinity-purified with Protein A Sepharose (Invitrogen) and eluted in 0.1 *M* glycine pH 3.0 in ten fractions, with each fraction containing 1 ml eluted protein. The eluted protein fractions were collected in 1.5 ml Eppendorf tubes containing 100 µl neutralizing buffer (600 m*M* Tris pH 7.4, 3 *M* NaCl). The final neutralizing buffer composition was thus 60 m*M* Tris pH 7.4, 300 m*M* NaCl. The tagged proteins were incubated with PreScission protease for 16 h at 4°C to remove the C-terminal Fc tag. PreScission protease was produced as a GST fusion in *Escherichia coli* BL21 (DE3) cells from the pGEX-6P-1 vector (Addgene). The cleaved Fc fusion protein was again affinity-purified with Protein A Sepharose, and the flowthrough containing the cleaved SALM3 LRR-Ig or PTPσ Ig1-3 was collected and purified by size-exclusion chromatography using Superdex 75 10/300 (GE Healthcare) for PTPσ Ig1-3 and Superdex 200 10/300 (GE Healthcare) for SALM3 LRR-Ig in 60 m*M* Tris pH 7.5, 300 m*M* NaCl (Fig. 1). Purified SALM3 LRR-Ig and PTPσ Ig1-3 were concentrated to 8–10 mg ml^{-1} with Amicon ultracentrifugal filter units (10 kDa molecular-mass cutoff; Merck).

2.3. Protein crystallization

For crystallization of the SALM3–PTPσ complex, SALM3 LRR-Ig (8 mg ml^{-1}) and PTPσ Ig1-3 (8 mg ml^{-1}) were mixed in a molar ratio of 1:1.2. The mixture was incubated at 4°C for 60 min before setting up crystallization experiments. Crystallization was carried out in MRC 96-well sitting-drop plates (Molecular Dimensions) using a Mosquito LCP nanodispensing robot (STP Labtech). We screened for crystallization of the complex using the Helsinki Random I and Helsinki Complex screens available at the Crystallization Core Facility, Institute of Biotechnology, University of Helsinki (https://www2.helsinki.fi/en/infrastructures/integrated-structural-cell-biology/sparse-matrix-screens) and the JCSG+, MIDAS and Morpheus crystallization screens (Molecular Dimensions). Initially, within one day of crystallization setup, thin needle-

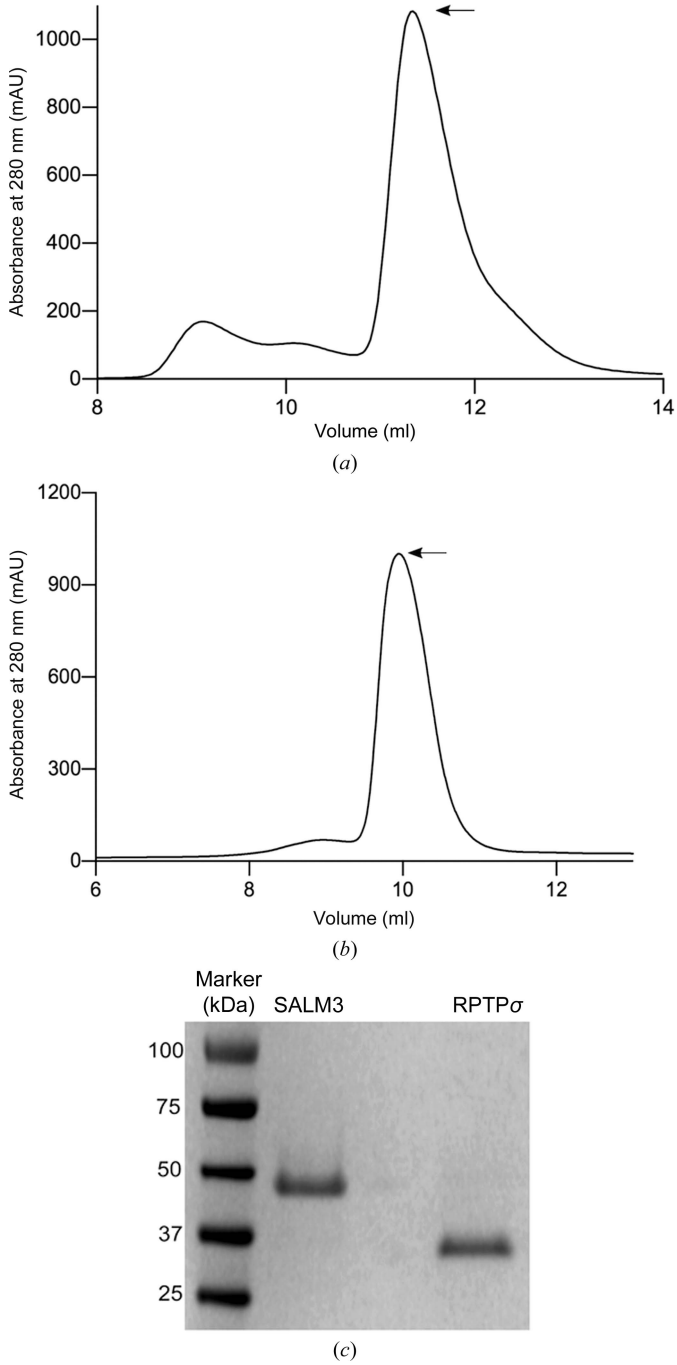

Figure 1
Purification of the SALM3 LRR-Ig and PTPσ Ig1-3 protein constructs. (*a*, *b*) Size-exclusion chromatography profiles of (*a*) the SALM3 LRR-Ig construct and (*b*) the PTPσ Ig1-3 construct. (*c*) SDS–PAGE of the purified proteins as labeled in the figure.

shaped SALM3–PTPσ crystals were obtained using the Helsinki Complex screen in a condition consisting of 0.1 *M* sodium acetate pH 4.5, 0.1 *M* magnesium acetate, 8% polyethylene glycol (PEG) 8000 (Fig. 2*a*) at 22°C. These crystals diffracted to a very low resolution of ∼20–25 Å. We then attempted to optimize the initial hit conditions using an additive screen (Hampton Research) and obtained larger thin needle-shaped or plate-shaped SALM3–PTPσ crystals from several conditions, but these also diffracted poorly. Further, we tried to optimize the crystals using a pH range from pH 4 to pH 8, crystallization temperatures of 22 and 4°C, different molecular-weight PEGs that included PEG 3350, PEG 4000, PEG 6000, PEG 8000 and PEG 10 000, and PEG concentrations from 4% to 15%. These optimization methods did not help to obtain protein crystals that diffracted to higher resolution. At this point, we scaled up to a drop size of 1 µl in 24-well plates at 4°C, which yielded more stable crystals.

The initial needle-shaped crystal contained magnesium acetate, so we replaced Mg^{2+} with other divalent metal ions, including Zn^{2+}, Mn^{2+} and Ca^{2+}, and monovalent metal ions, such as Na^{+}, NH_4^{+} and Li^{+}. Larger plate-like crystals were obtained in larger drops at 4°C using salts such as 0.05 *M* manganese acetate, 0.05 *M* zinc acetate and 0.05 *M* calcium acetate which diffracted to 8–9 Å resolution. We also attempted crystallization with deglycosylated protein, but this did not help to improve the resolution. We further replaced the acetate anion with anions such as Cl^{-}, NO_3^{-}, SO_4^{2-} and citrate ($C_6H_8O_7^{3-}$). We were able to obtain several larger crystals (0.2 × 0.2 × 0.2 mm) using the salts lithium nitrate, lithium sulfate, zinc sulfate, magnesium sulfate and calcium

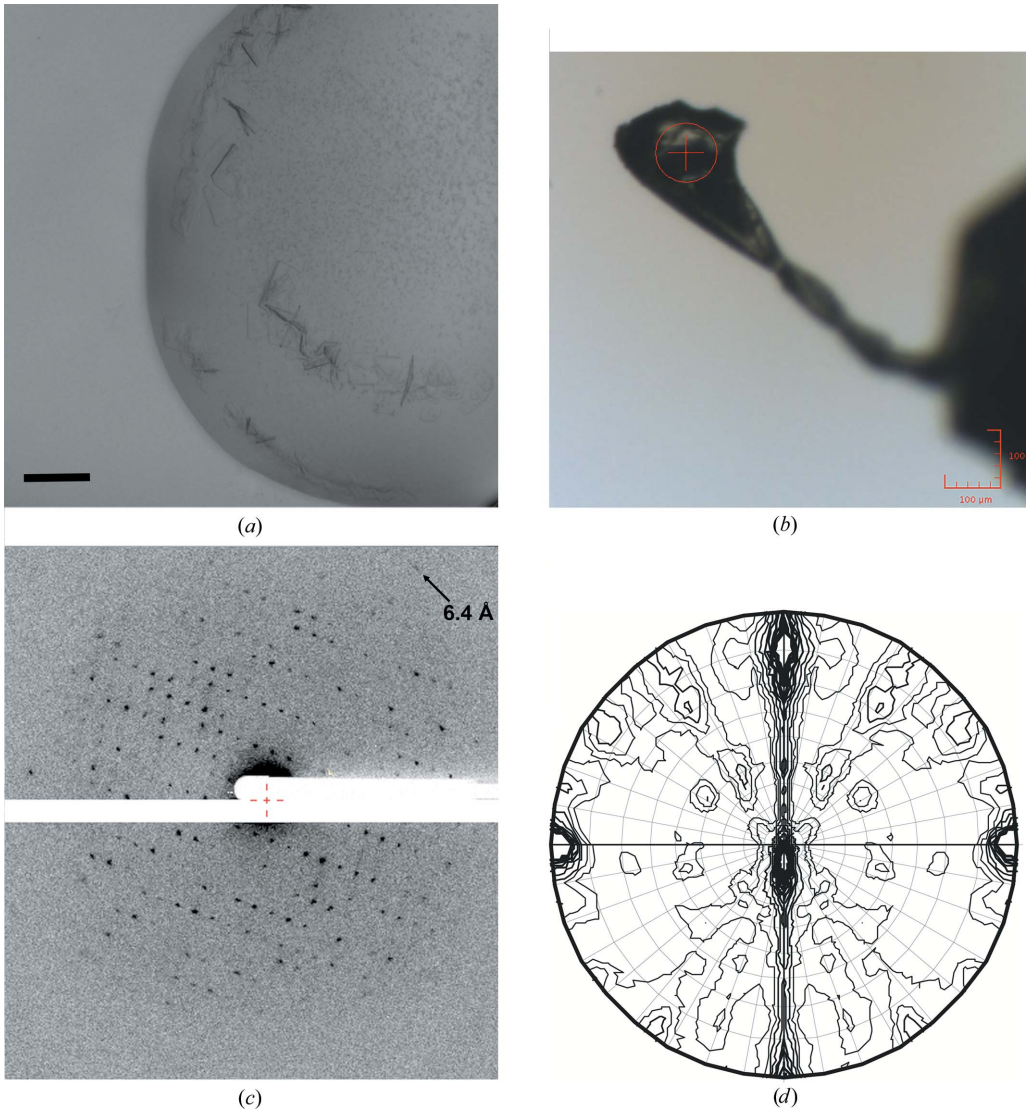

Figure 2
Crystallization and diffraction analysis of the SALM3–PTPσ complex crystals. (*a*) Initial hit from the 96-well screen. The scale bar corresponds to 100 µm. (*b*) Example of an optimized crystal mounted on a loop for data collection. (*c*) A diffraction pattern from the best crystal, with visible diffraction to 6.4 Å resolution in this orientation indicated by an arrow. (*d*) Self-rotation plot displayed at $\kappa = 180°$; the *C*2 crystallographic twofold peak is visible along the *y* axis, and the noncrystallographic peaks along the *x* axis of the plot as indicated in the text (at $\theta = 99.43°$, $\varphi = 0.0°$ and a symmetry-related peak at $\theta = 10.43°$, $\varphi = 0.0°$) are indicative of the presence of one dimer related by rotational symmetry in the asymmetric unit.

Table 2
Crystallization of the SALM3 LRR-Ig–PTPσ Ig1-3 complex.

Method	Sitting-drop vapor diffusion
Plate type	Cryschem 24-well sitting-drop plate (Hampton Research)
Temperature (K)	277
Protein concentration	8 mg ml^{-1} SALM3 LRR-Ig, 8 mg ml^{-1} PTPσ Ig1-3
Buffer composition	20 m*M* Tris pH 7.4, 100 m*M* NaCl
Crystallization reservoir solution	0.1 *M* sodium acetate pH 4.5, 0.05 *M* magnesium sulfate, 4% PEG 8000
Volume and ratio of the drop	1 µl, 1:1 ratio of protein and reservoir solution
Volume of reservoir (µl)	500

chloride. Finally, the best three-dimensional crystals were obtained with 0.1 *M* sodium acetate pH 4.5, 0.05 *M* magnesium sulfate, 4% PEG 8000, which diffracted to a resolution of 6.5 Å (Fig. 2; Table 2).

2.4. Data collection and processing

Data were collected at the Diamond Light Source (Didcot, Oxfordshire, UK) and ESRF (Grenoble, France) synchrotrons; the best data set was obtained on beamline ID23-1 at ESRF. Samples were cryoprotected with 15% ethylene glycol or 15% glycerol or were soaked in Paratone-N oil. The best data were collected from a crystal that was cryoprotected with 15% glycerol. A total of 180° of data (3600 images) were collected with 0.05° oscillation per frame and with a 0.02 s exposure time with 50% beam transmission (with a final flux of 4.25 × 10^{11} photons s^{-1} at the sample) at a wavelength of 0.873127 Å with a total exposure time of 72 s. The data were processed with *XDS* and *XSCALE* (Kabsch, 2010) and the crystal space group was determined to be *C*2, as described in Table 3.

Table 3
Data-collection and processing statistics.

Values in parentheses are for the highest resolution shell.

Diffraction source	ID23-1, ESRF
Wavelength (Å)	0.873130
Resolution range (Å)	50–6.5
Space group	*C*2
a, *b*, *c* (Å)	211.4, 121.5, 134.0
α, β, γ (°)	90.0, 126.8, 90.0
Rotation range per image (°)	0.05
Exposure time per image (s)	0.02
Total No. of reflections	16313
No. of unique reflections	5337
Multiplicity	3.1 (2.6)
Completeness (%)	96.7 (84.8)
Mean $I/\sigma(I)$	9.7 (0.87)
$R_{\rm merge}$ (%)	5.3 (126.1)
$R_{\rm meas}$ (%)	6.5 (155.0)
$R_{\rm p.i.m.}$ (%)	5.1 (65.7)
$CC_{1/2}$ (%)	99.8 (55.5)
$R_{\rm work}/R_{\rm free}$ (%)	31.6/38.2
Average *B* factor (Å^2)	560.3
Ramachandran plot (%)	
Favored	93.7
Allowed	5.93
Outliers	0.37

3. Results and discussion

The structure of the SALM5 LRR-Ig–PTPδ Ig1-3 complex has previously been solved (Lin *et al.*, 2018; Choi *et al.*, 2016). SALM5 LRR-Ig and PTPδ Ig1-3 have 41.8% and 69.6% sequence identity to the SALM3 LRR-Ig and PTPσ Ig1-3 constructs, respectively. Here, we present the initial crystallization and structure solution of SALM3 in complex with PTPσ. In our hands, the best expression of the vertebrate cell-surface LRR proteins was obtained from *Drosophila* S2 cells, from which we purified both of the proteins with typical final yields of ∼4 mg l^{-1} for SALM3 and ∼12 mg l^{-1} for PTPσ. Protein A affinity purification coupled with SEC purification after PreScission protease cleavage of the C-terminal Fc tag typically yielded >90% pure monodisperse protein. The optimization yielded large (>200 mm) crystals, but from the diffraction experiments it was clear that the crystals were not well ordered and that the solvent content was quite high. Calculated possible options given space group *C*2 suggested either one 2:2 complex of SALM3–PTPσ with a Matthews coefficient of 4.95 Å^3 Da^{-1} or two complexes with a Matthews coefficient of 2.46 Å^3 Da^{-1}, corresponding to 75.2% and 50.4% solvent content, respectively. The self-rotation function plot, with one major peak for a noncrystallographic twofold at polar coordinates 99.43°, 0.0°, 180° (Fig. 2), suggests that one 2:2 complex is most likely to be present in the asymmetric unit. The low-resolution structure of SALM3–PTPσ was solved by molecular replacement with *Phaser* (McCoy *et al.*, 2007) using the previously solved SALM3 LRR dimer structure (PDB entry 6tl8; Karki *et al.*, 2020) and the PTPδ Ig1-3 domain coordinates from the structure of the SALM5 complex (PDB entry 5xnp; Lin *et al.*, 2018) as search models. *Phaser* was able to find the LRR domain dimer and individually place two PTPδ Ig1-3 monomers in the same positions on both sides of the LRR dimer, as expected from the known structure of the dimeric SALM5 complex. Thus, the molecular-replacement results confirmed the presence of one 2:2 dimer in the asymmetric unit. Visualization of the crystal packing supports the correctness of the solution (Supplementary Fig. S1).

The initial solution at 6.5 Å resolution had translation-function *Z*-scores of 10, 9.5 and 8.7 for each fitted molecule, an overall log-likelihood gain of 225 and *R* factors $R_{\rm work}$ and $R_{\rm free}$ of 41.9% and 45.7%, respectively, after initial refinement with *REFMAC* (Murshudov *et al.*, 2011). The best refinement results were obtained using the *LORESTR* protocol in *CCP*4 (Kovalevskiy *et al.*, 2016) with external restraints from six homologous structures refined at better than 3.5 Å resolution and jelly-body refinement, resulting in an $R_{\rm work}$ and $R_{\rm free}$ of 31.6% and 38.2%, respectively, indicating a clear solution, and a closely matching complex organization compared with that of SALM5–PTPδ was found with individually placed protein components (Fig. 3). However, despite effort, placement of the SALM3 Ig domain between the PTPσ Ig2 and Ig3 domains was not possible at this resolution through molecular replacement, perhaps owing to the limited data quality, although limited residual difference density was visible in the maps. Hence, it was not possible to model detailed interactions or refine the structure further, but only to obtain an initial

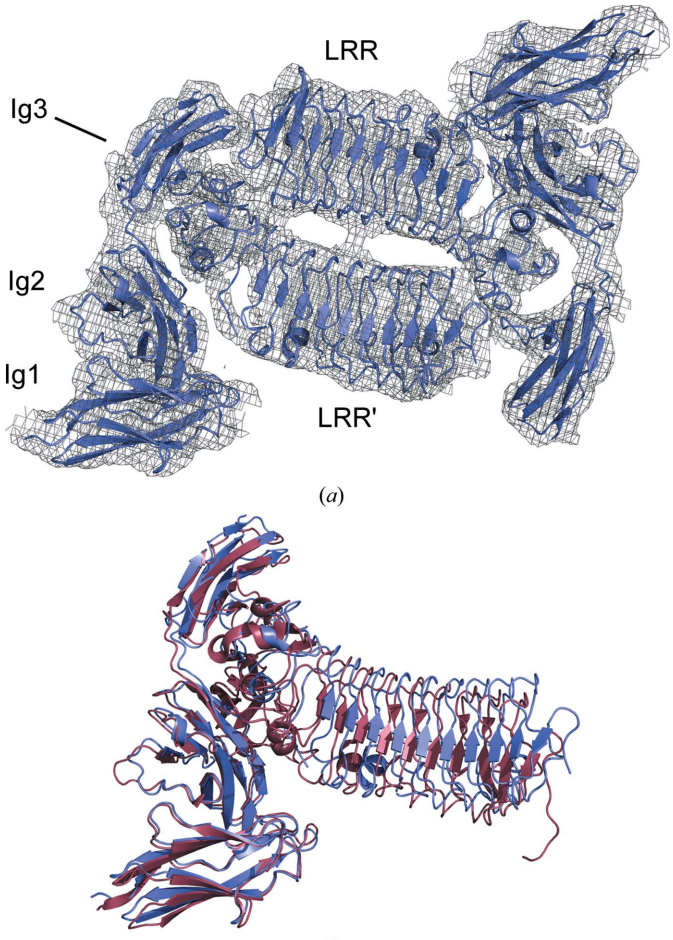

Figure 3
The preliminary structure of the SALM3–PTPσ complex. (*a*) Placement of the proteins. LRR and LRR′ denote the LRR domains of the SALM3 dimer; the PTPσ Ig1-3 domains are indicated and are visible on each side of the SALM3 dimer. A composite omit map at the 1σ contour level is displayed on the complex. (*b*) Alignment of the SALM3 complex (blue) with the monomeric SALM5 complex (dark red). For simplicity the whole 2:2 dimer is not shown here.

structure solution verifying the crystal contents and the overall organization of the SALM3 LRR domains relative to the PTPσ Ig domains. The crystal diffraction was also found to be quite anisotropic, as analyzed by the *STARANISO* server (https://staraniso.globalphasing.org/cgi-bin/staraniso.cgi; Vonrhein *et al.*, 2018), with data to 5.9 Å resolution in the best direction and to 7.2 Å resolution in the worst direction; however, using anisotropically processed data in molecular replacement or refinement did not improve the statistics or the map quality, and thus in the end the non-manipulated data were used for simplicity. Further optimization of the crystals will be needed to push the resolution further in order to refine the structure at higher resolution. However, the current structure solution verifies our earlier overall observation based on SEC-SAXS modeling that SALM3 forms a ligand complex similar to that of SALM5 with the presynaptic PTPσ (Karki *et al.*, 2020), and therefore it is probable that they have similar and synergistic functions (Li *et al.*, 2015; Choi *et al.*, 2016).

Acknowledgements

We thank Dr Violeta Manole for help with protein crystallization. All crystallization experiments were performed at the INSTRUCT-HiLIFE crystallization core facility, a member of FINSTRUCT and Biocenter Finland. Diffraction data were collected on ESRF beamline ID23-1 and we are grateful to the ESRF staff for their help with remote data collection.

Funding information

This work was supported by grants from the Jane and Aatos Erkko Foundation (to TK) and the Magnus Ehrnrooth Foundation (to SK).

References

Bunch, T. A., Grinblat, Y. & Goldstein, L. S. (1988). *Nucleic Acids Res.* **16**, 1043–1061.
Choi, Y., Nam, J., Whitcomb, D. J., Song, Y. S., Kim, D., Jeon, S., Um, J. W., Lee, S.-G., Woo, J., Kwon, S.-K., Li, Y., Mah, W., Kim, H. M., Ko, J., Cho, K. & Kim, E. (2016). *Sci. Rep.* **6**, 26676.
Craig, A. M. & Kang, Y. (2007). *Curr. Opin. Neurobiol.* **17**, 43–52.
Gorlewicz, A. & Kaczmarek, L. (2018). *Front. Cell. Dev. Biol.* **6**, 119.
Han, K. A., Jeon, S., Um, J. W. & Ko, J. (2016). *Int. Rev. Cell. Mol. Biol.* **324**, 39–65.
Kabsch, W. (2010). *Acta Cryst.* D**66**, 133–144.
Karki, S., Paudel, P., Sele, C., Shkumatov, A. V. & Kajander, T. (2018). *Protein Eng. Des. Sel.* **31**, 147–157.
Karki, S., Shkumatov, A. V., Bae, S., Kim, H., Ko, J. & Kajander, T. (2020). *Sci. Rep.* **10**, 11557.
Ko, J., Kim, S., Chung, H. S., Kim, K., Han, K., Kim, H., Jun, H., Kaang, B. & Kim, E. (2006). *Neuron*, **50**, 233–245.
Kovalevskiy, O., Nicholls, R. A. & Murshudov, G. N. (2016). *Acta Cryst.* D**72**, 1149–1161.
Laurén, J., Airaksinen, M. S., Saarma, M. & Timmusk, T. (2003). *Genomics*, **81**, 411–421.
Leshchyns'ka, I. & Sytnyk, V. (2016). *Neural Plast.* **2016**, 6427537.
Li, Y., Zhang, P., Choi, T. Y., Park, S. K., Park, H., Lee, E. J., Lee, D., Roh, J. D., Mah, W., Kim, R., Kim, Y., Kwon, H., Bae, Y. C., Choi, S. Y., Craig, A. M. & Kim, E. (2015). *Cell. Rep.* **12**, 1618–1630.
Lin, Z., Liu, J., Ding, H., Xu, F. & Liu, H. (2018). *Nat. Commun.* **9**, 268.
Mah, W., Ko, J., Nam, J., Han, K., Chung, W. S. & Kim, E. (2010). *J. Neurosci.* **30**, 5559–5568.
McCoy, A. J., Grosse-Kunstleve, R. W., Adams, P. D., Winn, M. D., Storoni, L. C. & Read, R. J. (2007). *J. Appl. Cryst.* **40**, 658–674.
Medina-Cano, D., Ucuncu, E., Nguyen, L. S., Nicouleau, M., Lipecka, J., Bizot, J.-C., Thiel, C., Foulquier, F., Lefort, N., Faivre-Sarrailh, C., Colleaux, L., Guerrera, I. C. & Cantagrel, V. (2018). *eLife*, **7**, e38309.
Missler, M., Südhof, T. C. & Biederer, T. (2012). *Cold Spring Harb. Perspect. Biol.* **4**, a005694.
Murshudov, G. N., Skubák, P., Lebedev, A. A., Pannu, N. S., Steiner, R. A., Nicholls, R. A., Winn, M. D., Long, F. & Vagin, A. A. (2011). *Acta Cryst.* D**67**, 355–367.
Nam, J., Mah, W. & Kim, E. (2011). *Semin. Cell Dev. Biol.* **22**, 492–498.
Reissner, C., Runkel, F. & Missler, M. (2013). *Genome Biol.* **14**, 213.
Seiradake, E., Coles, C. H., Perestenko, P. V., Harlos, K., McIlhinney, R. A., Aricescu, A. R. & Jones, E. Y. (2011). *EMBO J.* **30**, 4479–4488.
Um, J. W. & Ko, J. (2013). *Trends Cell Biol.* **23**, 465–475.
Ushkaryov, Y. A., Petrenko, A. G., Geppert, M. & Südhof, T. C. (1992). *Science*, **257**, 50–56.
Vonrhein, C., Tickle, I. J., Flensburg, C., Keller, P., Paciorek, W., Sharff, A. & Bricogne, G. (2018). *Acta Cryst.* A**74**, a360.
Yamagata, M., Sanes, J. R. & Weiner, J. A. (2003). *Curr. Opin. Cell Biol.* **15**, 621–632.